CONTENTS

I. INTRODUCTION AND MOTIVATION

The Triangle Universities Nuclear Laboratory (TUNL) is home to the University of North Carolina-Chapel Hill's Laboratory for Experimental Nuclear Astrophysics (LENA). The facility is discussed in detail by Cesaratto et al. [7]. The focus and speciality of LENA is to measure γ-ray spectra of astrophysically significant, low-energy nuclear reactions. These spectra can be used to calculate branching ratios, cross sections, and reaction rates. An example of such a measurement made recently at LENA is the $^{18}\mathrm{O}(p,\gamma)^{19}\mathrm{F}$ reaction [5]. The cross sections of such reactions are very small at the energies present in thermonuclear fusion. A useful figure of merit describing the signal-to-noise for direct measurements is the

following, given by Champagne et al. [8]

$$F.O.M. = \frac{\text{signal rate}}{\sqrt{\text{background rate}}} \tag{1}$$

Since this figure of merit increases linearly with signal rate, and only as the reciprocal of the square root of background rate, one may be tempted to fully invest in the highest possible signal rate while neglecting to decrease background rate. However, this works only up to a point, since targets are easily damaged by too large an ion beam current. Therefore, effective measurement of γ-ray spectra at these energies requires two special considerations: a high-intensity proton beam and careful reduction of counts from background sources.

Of the two ion sources at LENA, the Electron Cyclotron Resonance (ECR) ion source is the more intense. The original acceleration column was able to produce a DC proton beam on target of approximately 2 mA, which provided the requisite high-intensity beam and facilitated several important measurements [5] [6]. However, lossy beam-transport exacerbated several beam-transport difficulties which reduced the beam current arriving on target and ultimately caused damage to the acceleration column itself. The first portion of this thesis describes work performed to improve the beam transport efficiency.

The γ-ray spectrometer at LENA utilizes a sophisticated coincidence detection scheme to reduce the radiation background. Details can be found in Longland et al. [9] Nevertheless, further reduction of background counts is desirable to improve the signal-to-noise ratio. The second portion of this thesis describes work performed to quantify the improvement in measurement signal-to-noise by implementing a new method for operating the ECR ion source.

The strategy for further reducing background counts implemented at LENA involves changing from a DC beam regime to a pulsed ion beam. Specifically, we desired a beam of 10% duty cycle, with 100 ms of beam on target followed by 900 ms of no beam. A software gate in LENA's data acquisition software, JAM [10], is then used to differentiate spectra obtained when the beam is on from spectra obtained when the beam is off. This method has been successfully implemented, with results discussed below.

Pulsing of the beam at 10% duty cycle is is equivalent to a 90% reduction in beam current. The DC beam current must then be increased by a factor of ten, to roughly 20 mA, to maintain an average beam current of approximately 2 mA when the beam is pulsed. This increase in DC beam current will be achieved with a newly constructed accelerator column,

which is an ongoing project.

II. ION BEAM-TRANSPORT IMPROVEMENTS

In addition to the newly constructed accelerator column for the ECR source, adjustments of the ion beam transport at LENA were necessary to achieve the desired increase in beam current reaching the target. The new column will transport an ion beam with a larger diameter than the old column, but a 1" vertical aperture constraint at the bending magnet still remains. Previously, the quadrupole magnetic lens located between the ECR and bending magnet squeezed the beam into an eccentric ellipse that was just vertically narrow enough to pass through the bending magnet, but its horizontal divergence was too large to be completely focused on the target by the second quadrupole lens. This resulted in an unacceptable loss of beam current. Fig. 1 shows an overhead, schematic view of the laboratory in its old configuration.

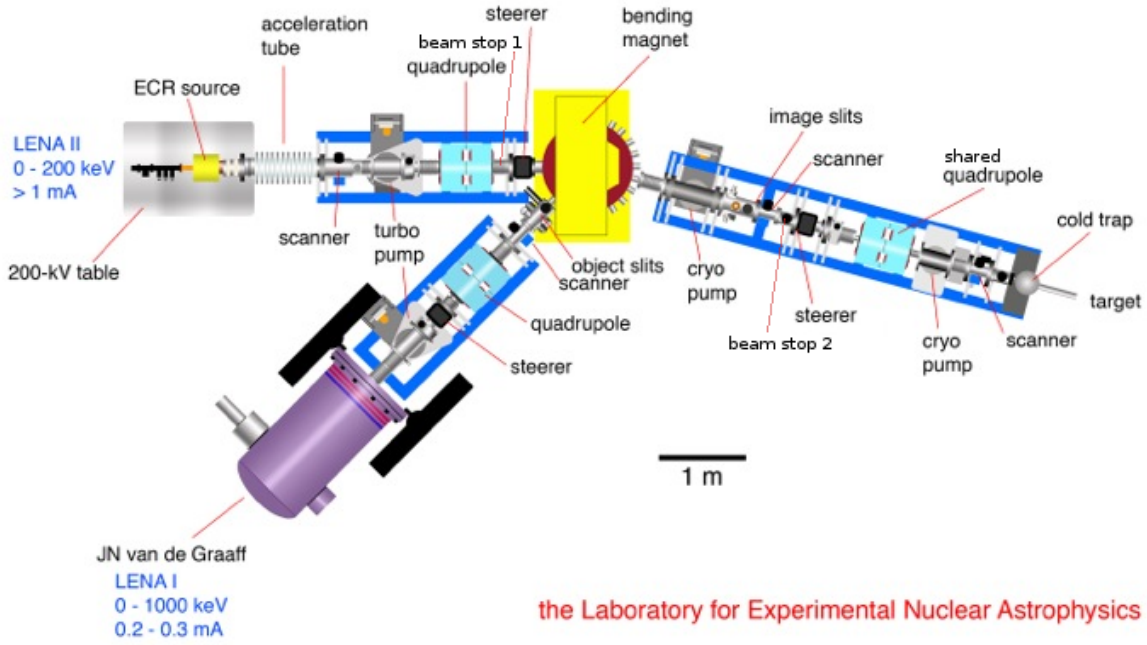

FIG. 1: An overhead schematic view the old laboratory setup [8]. The ion beam is produced by the ECR source and travels from left to right, first passing through a quadrupole lens (shown in light blue). After passing through the bending magnet (shown in yellow), the ion beam is focused by another quadrupole lens onto the target. Note the positions of beam stops 1 and 2, which will be referenced later.

To overcome this problem, solenoidal lenses will be used to focus the beam along the ECR beam line instead of quadrupole lenses. Solenoidal lenses are advantageous, because unlike the quadrupole lenses, they focus the beam with axial symmetry. Solenoidal lenses will also be able to accommodate the increase in beam diameter as it emerges from the new accelerator column. Overall, transport efficiency will be greatly increased with these lenses.

At LENA, the ion beam current is measured using instruments called beam stops. These devices work by interrupting the path of the ion beam with a plate of conducting material that is separated from the ground potential by an insulator. The current is then measured directly from this conductor. The installation of the new acceleration column at LENA introduces an additional problem. The beam stops in the old laboratory setup of Fig. 1 lack the water cooling to withstand the higher ion beam current without being damaged, and they are too small to fully interrupt the ion beam. With that in mind, new beam stops had

to be designed so that ion beam current could be measured in the new laboratory setup. Fig. 2 shows a schematic view of the laboratory with the new solenoids and new beam stops.

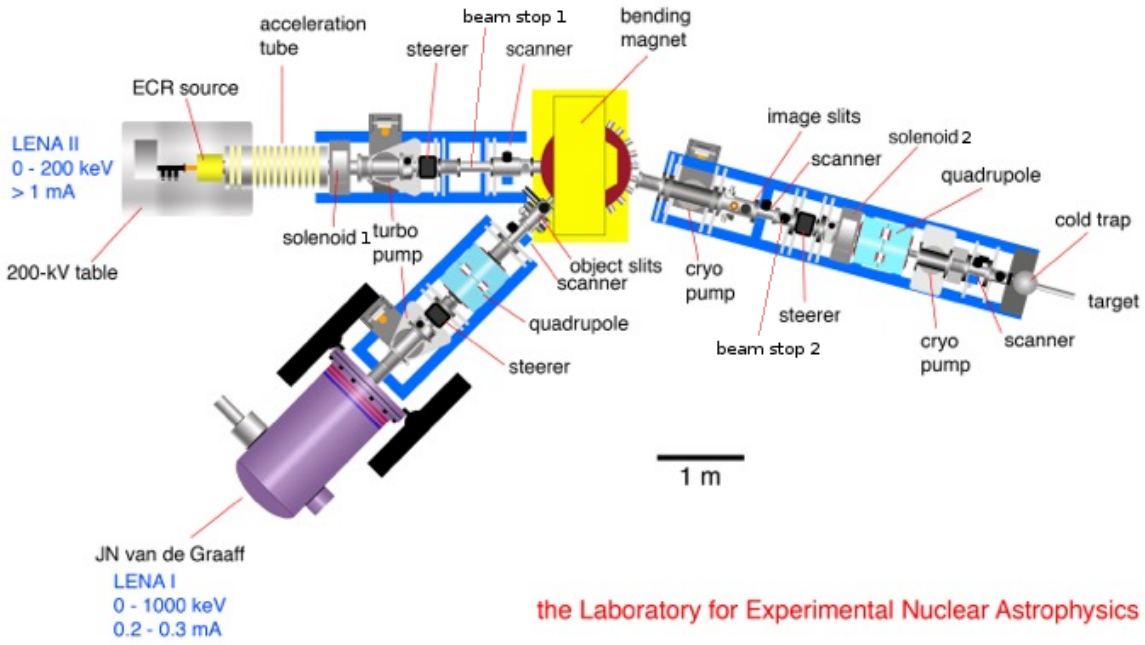

FIG. 2: An overhead schematic view the new laboratory setup [8]. The column and beam stops have been replaced by upgraded versions, which will be discussed below. The first quadrupole lens has been removed entirely, and two solenoidal lenses have been introduced. Note the placement of the beam stops and solenoids, as they will be referenced later.

Solenoids

The quadrupole lens that exclusively served the ECR beam has been removed entirely, but the quadrupole lens that is currently shared by the ECR beam and the JN Van de Graaff beam must remain in place to focus the JN beam. The first solenoidal lens has been placed immediately at the end of the ECR column. With this placement, the beam can be focused to a 1" diameter waist located at the bending magnet. After leaving the bending magnet, the beam will diverge slowly enough to be captured fully by the second solenoidal lens, which has been placed just before the shared quadrupole lens. This solenoidal lens will then focus the entire beam on target.

The solenoidal lenses are each comprised of eight separate, resin-encased coils of hollow copper tubing with a cross-sectional area of 36 mm^2. Each of the coils has an inner diameter of 10", an outer diameter of 20", and is 0.7" thick. Current flows in series through the eight coils in the lens, but each coil receives its own inlet and outlet for chilled water. This chilled water flows through the hollow copper tubes and carries away the heat caused by the current.

The necessary maximum magnetic field required for focusing the beam is 0.134 T at the center of the lens and 0.082 T at the outer edge. The required current to produce this field is 80 A. The eight coils have a series resistance of 0.168 Ω, so a voltage of 13.4 V is required to produce the needed current.

Given the relatively large magnetic field produced by these lenses, a high-permeability flux return casing is needed to ensure that the field is as closely contained as possible. My specific role in the implementation of the solenoidal lenses was the design of this flux return casing and the mounting system. The flux return casing consists of two 21" × 21" × 0.75" plates of cold-rolled steel on either side of the coils. These plates have a 6.5" diameter hole cut in their center to allow for 6" diameter Dependex tubing to pass through. The two plates are bolted together by eight 6" × 7.75" × 0.75" bars of cold-rolled steel. Aluminum cases hold the coils within this flux return.

Once placed in their flux return casings, the lenses were mounted on the pre-existing Unistrut supports at LENA. Two bars of aluminum span the two Unistruts and 0.5" foot screws are screwed upward through these bars. Two steel bars on the faces of the flux return casings rest on top of these foot screws, and the adjustment of the screws allowed the lenses to be moved up and down for alignment. Through the front of these aluminum bars, 0.375" foot screws were inserted to allow for forward and backward adjustment of the lens position. Also attached to the Unistruts were two pieces of angle iron on either side of the lens, through which 0.375" foot screws were also inserted. These allowed for horizontal alignment. Currently, both solenoidal lenses have been successfully aligned. Fig. 3 shows a schematic view of the solenoids. Fig. 4 and Fig. 5 show solenoid 1 and solenoid 2, respectively, installed in the beam line.

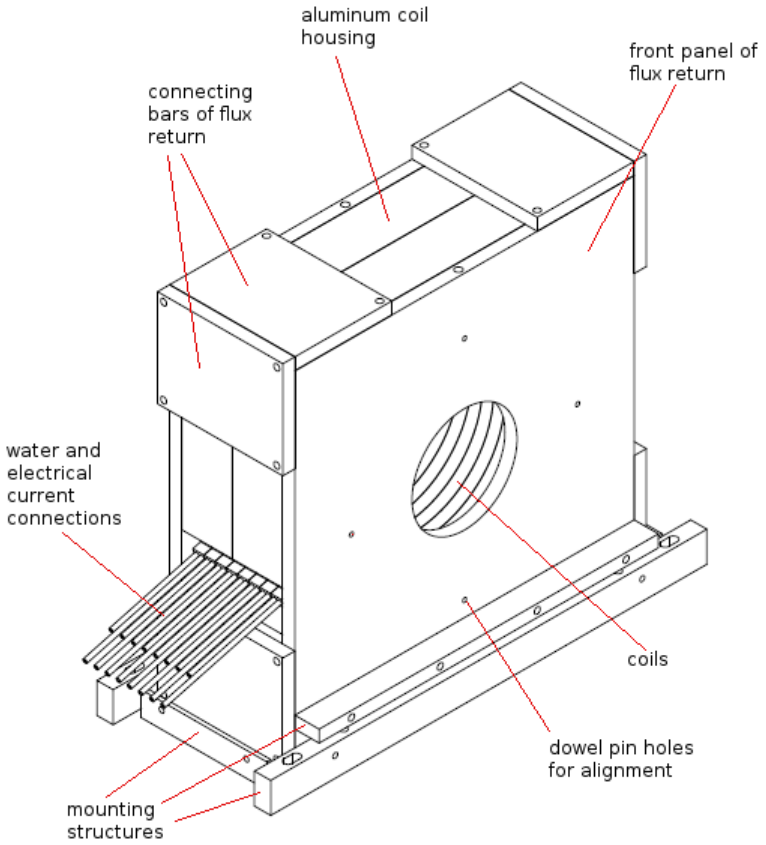

FIG. 3: A schematic view of one of the solenoidal lenses, with flux return and mounting. Each of the copper tubes labeled in the image as "water and electrical current connections" serves as *both* a water *and* electrical connection. The electrical connections are connected in series, while the water cooling connections are connected in parallel. The dowel pin holes allow thin wire to be attached to the front and back faces of the lens in cross-hair formation to allow for laser alignment.

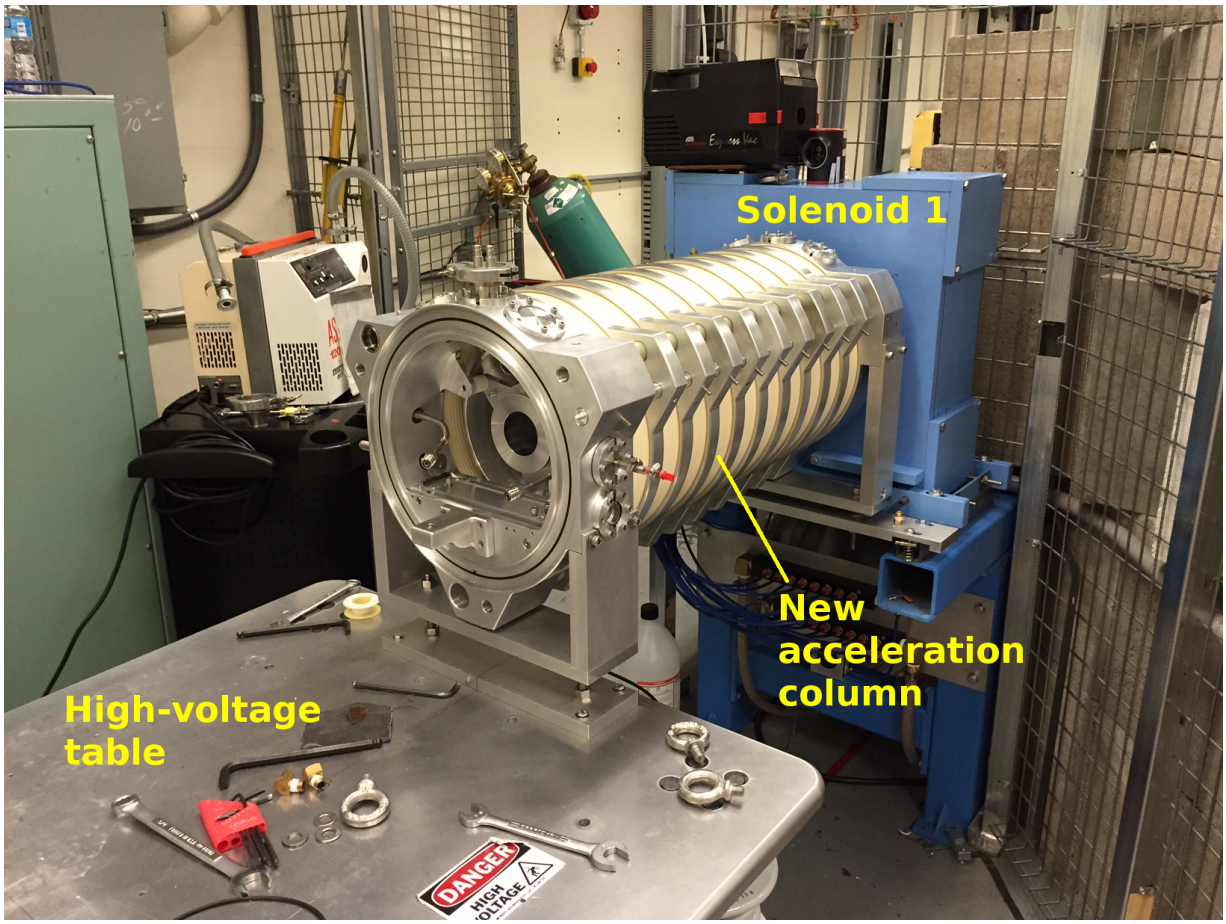

FIG. 4: The first solenoid installed at the ground potential end of the new accelerator column. This solenoid is "solenoid 1" in Fig. 2. The high-voltage table will house the microwave source and controlling electronics, and the open end of the column will be attached to the microwave source.

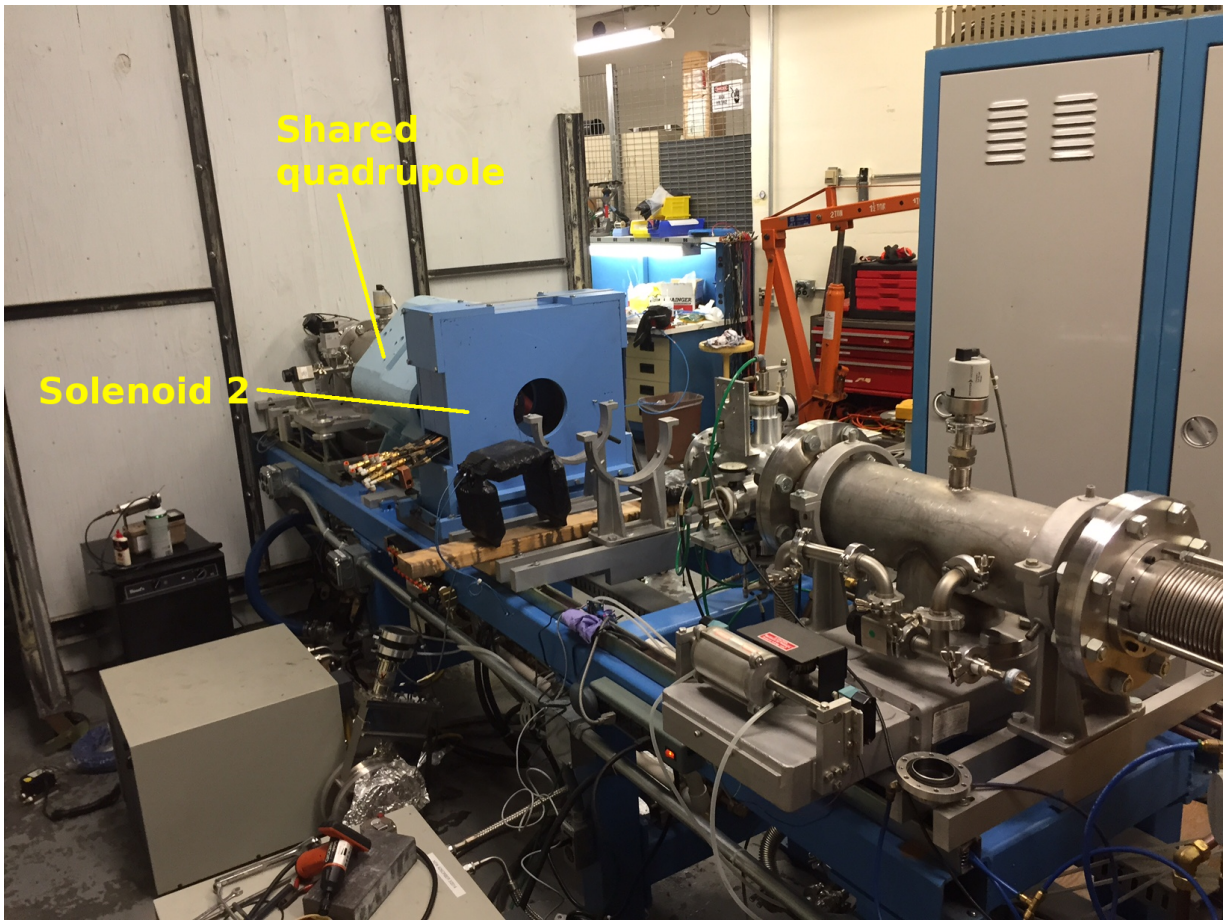

FIG. 5: The second solenoid lens installed in front of the shared quadrupole lens. The placement of these lenses in the beam-line can be seen in Fig. 2.

Beam stops

At maximum power, the proton beam produced by the new ECR acceleration column is expected to be between 5 kW and 7 kW. No beam stop currently available at LENA will withstand such power. To measure the beam current, a new beam stop was designed.

I completed the design of these beam stops based on a modification of the 2" beam stops currently used at TUNL. The most prominent feature of the new design is the 3" $\times$ 3" $\times$ 1.5" oxygen-free copper plate that creates the surface the beam will strike. This plate has a 0.25" wide, 0.375" deep spiral shaped groove with 0.0625" thick walls separating the groove. A second 3" $\times$ 3" $\times$ 1.5" copper plate has been brazed to the grooved plate with a 72% silver, 28% copper brazing alloy. This second copper plate has a 0.375" diameter tube through

which chilled, deionized water will flow from the top to the center. Water will then enter the center of the first plate and spiral outward, carrying heat with it. Fig. 6 shows the distinctive spiral groove of the beam stop. Fig. 7 shows the internal paths for water cooling in the beam stop.

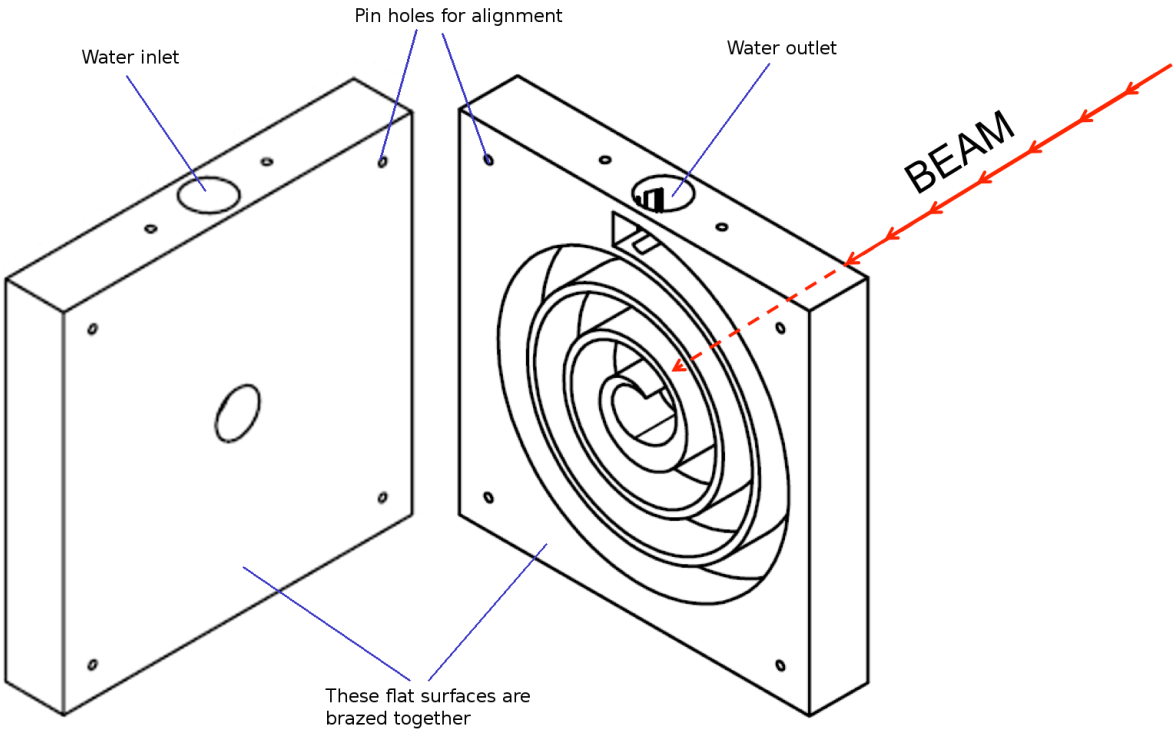

FIG. 6: The spiral shaped groove in the plate of the beam stop. The outside of the plate, where the beam strikes is just a flat surface. Oxygen-free copper pegs were inserted into the pin holes for aligning the plates during the brazing process.

The new beam stops fit within machined aluminum blocks that have been inserted between two sections of 4" diameter Dependex tubing by way of clamp flanges. Within the Dependex tubing that precedes the housing rests a 3.5" diameter, 3.5" long, thin cylindrical metal electrode that is held in place with six insulating pegs of Delrin acetal resin. This electrode will then be held at a voltage of -300 V. The purpose of this electrode is to repel any secondary electrons that are ejected from the surface of the copper plate, so that an accurate measurement of beam current may be made. An aperture of 2.5" inner diameter rests in front of this electrode. Currently, the two beam stops have been constructed and are

installed at LENA. Fig. 8 shows one of the assembled beam stops, just prior to installation. Fig. 9 shows a beam stop installed in the beam line.

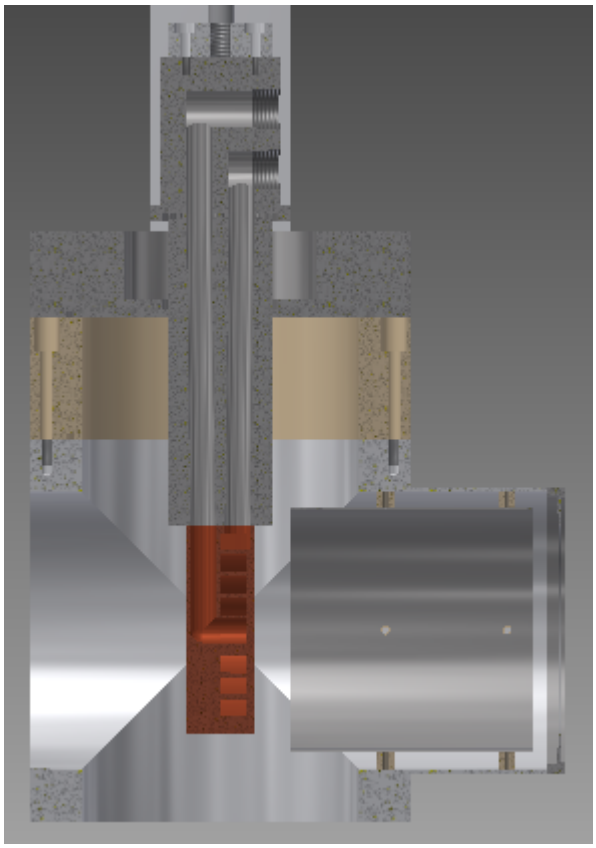

FIG. 7: A cross section of the beam stop in its down position, showing the internal paths for water cooling. In this image, the beam travels from right to left.

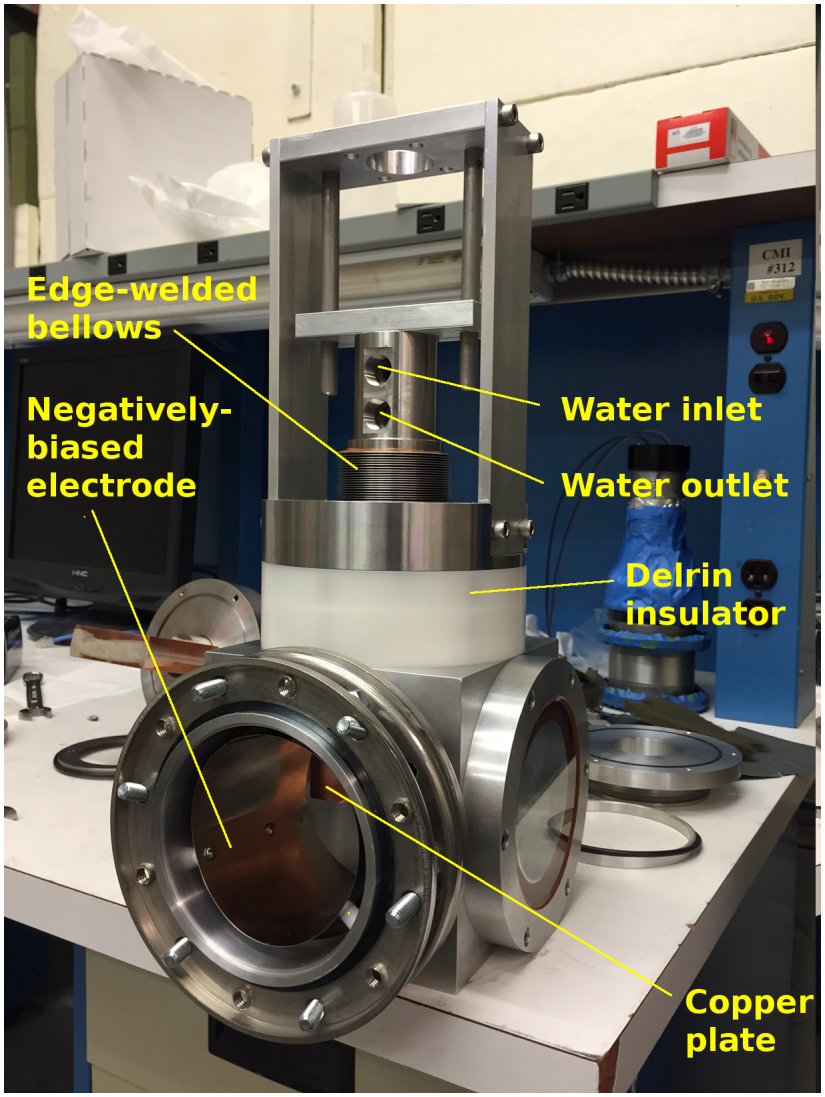

FIG. 8: One of the two assembled beam stops, before installation. The negatively biased electrode can be seen within. The assembly is seen here without the pneumatic actuator.

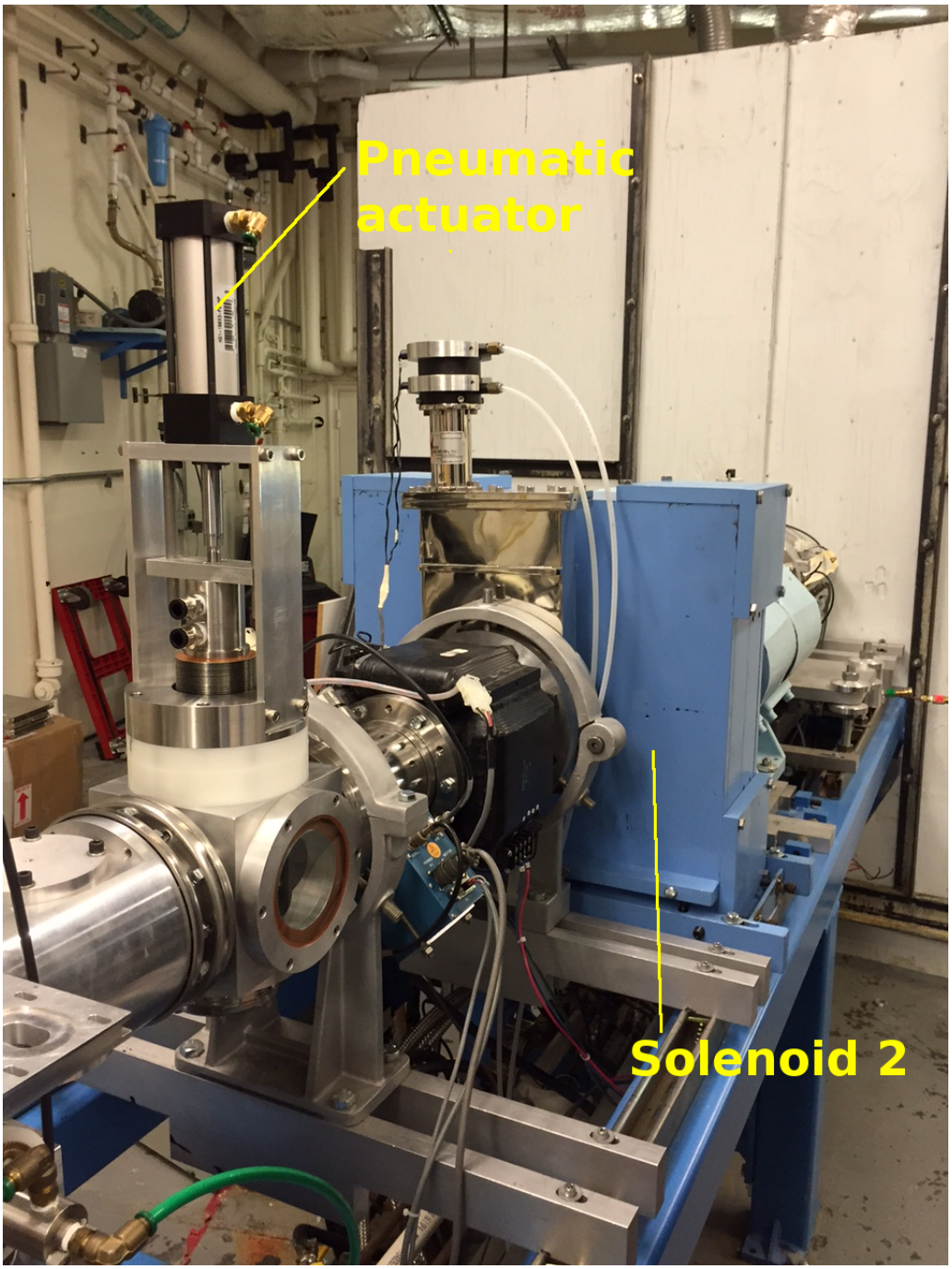

FIG. 9: The same solenoid as in figure 5, now with the second beam stop installed in front of it. The pneumatic actuator has been installed atop the beam stop, but the cooling water lines have not yet been connected.

III. ION BEAM-PULSING METHOD

During normal, DC operation of the ECR source, a constant voltage is used to power the microwave source. A three-stub tuner is used to minimize the reflected power of the microwave source. This minimization ensures that we have achieved the maximum power transfer from the microwave source to the plasma chamber [7]. The current to the lenses and the current to the steering magnets are then adjusted to achieve maximal beam on target. Pulsing the beam and acquiring useful data, however, requires special hardware and special procedures.

Hardware and control

Before the installation of the beam-transport hardware mentioned above, we created and tested the the beam-pulsing system. A National Instruments FieldPoint FP-1601 network module [1] was used in conjunction with a FieldPoint FP-PG-522 pulse generator [2] to produce the pulses. I wrote a LabView graphical user interface (GUI) to control the pulse generator from the LENA control room. The GUI allows for arbitrary on and off time, so that any duty cycle can be achieved. Powered by a 5 V source at each end, an optical fiber connection attaches the FieldPoint pulsing module to the ECR's microwave source, where the microwave pulses excite the plasma. Figure 10 shows the pulse signal after it has been passed through the optical fiber.

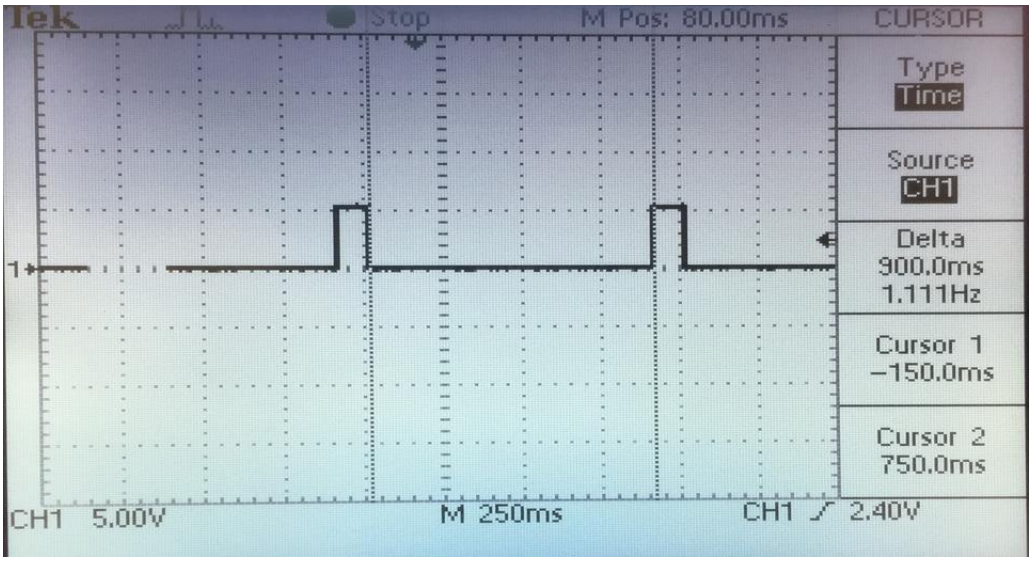

FIG. 10: An image of the oscilloscope display showing the voltage output of the pulsing signal. The pulse width amounts to 100 ms and the period amounts to 1000 ms, corresponding to a duty cycle of 10%.

After passing through the optical fiber, the pulsed voltage seen in Fig. 10 was used to drive the microwave source. To test that the source was was successfully pulsed and a pulsed beam was produced, we wanted to be able to measure the beam intensity as a function of time. For testing purposes, alligator clips were connected to the existing beam stop, and a long coaxial cable was wired to the control room. This cable attached to an oscilloscope through a resistor so that the voltage read by the oscilloscope was proportional to the beam current on the beam stop. After the ion beam was tuned for maximal DC beam current, the pulsing was turned on for the first time.

Initially, there were problems with the stability of the plasma. The shape of the pulse was not square as expected. Fig. 11 shows the signal on the beam stop. Furthermore, the plasma suffered from instabilities that prevented the pulsing from achieving more than a few cycles. Several options were considered for stabilizing the beam, including mixing argon with the hydrogen gas that is pumped into the plasma chamber. This was suggested by Art Champagne, and was pursued by Keegan Kelly, Bret Carlin, and Brian Walsh. However, this method did not solve the problem with the instability, and in fact it tended to extinguish the plasma even more readily. Therefore, the argon-hydrogen gas mixture idea was abandoned in favor of pure hydrogen.

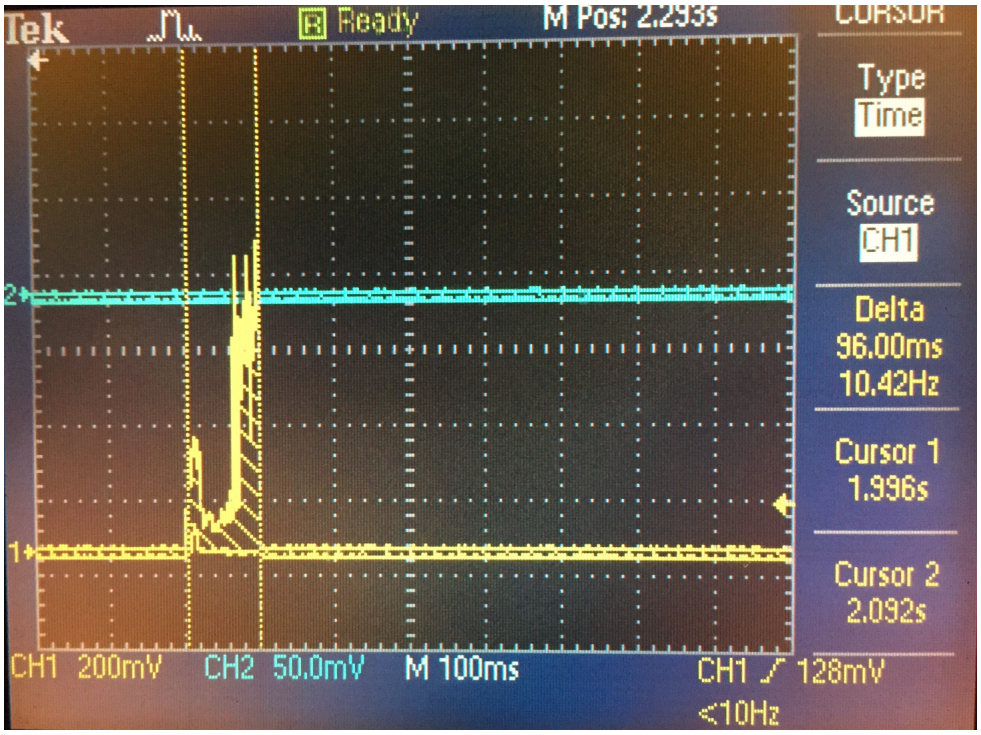

FIG. 11: Channel 1 (the yellow trace) shows the problem with ion beam stability prior to adjustment of the reflective power. Channel 2 (the light blue trace) shows the voltage of the DC beam current, before pulsing was turned on.

Keegan Kelley discovered that the instability could be resolved by adjusting the three-stub tuner to a mode away from the minimum reflected microwave power. In doing so, a stable pulsed beam was achieved. Fig. 12 and Fig. 13 show the oscilloscope display of successful beam pulsing, as measured using beam stop 1 from Fig. 1.

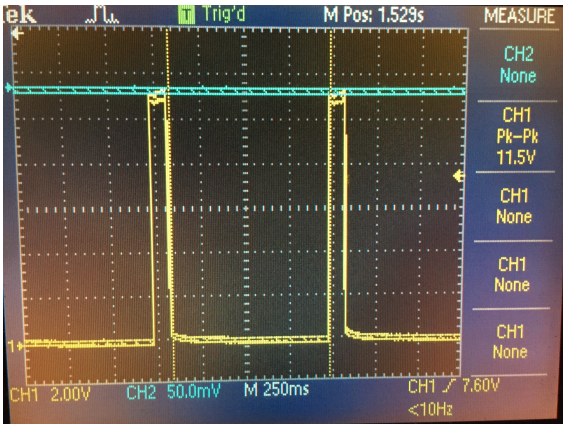

FIG. 12: Two pulses of the ion beam, shown here with 100 ms beam on and 900 ms beam off. One division of the x-axis corresponds to 250 ms.

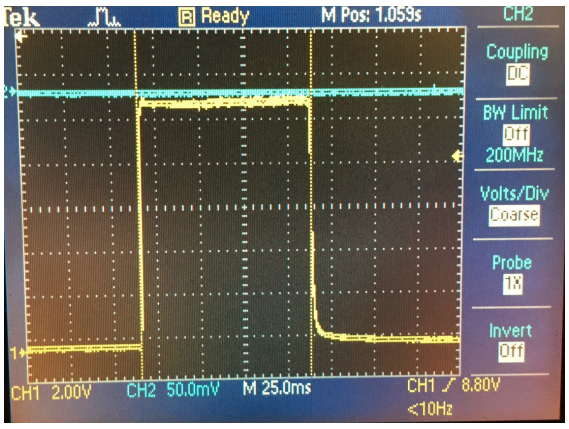

FIG. 13: A close up of the beam-on period. Note the flatness of the 100 ms wide signal, as well as the quick rise and fall times.

Data acquisition

Once the beam had been successfully pulsed, a method was needed for separating the spectra collected while the beam was on from the spectra obtained while the beam was off. LENA's data acquisition (DAQ) software, JAM [10], works by creating an "event" file that contains the entire energy and timing information for the radiation recorded by the γ-ray detector. In this context, radiation refers to the photons emitted by the nuclear reaction of astrophysical interest, and to photons arising from environmental background (e.g., ^{40}K and ^{208}Tl). Software conditions can be imposed on the events. In other words, only those events satisfying a given "software gate" (e.g., beam-on or beam-off events) can be sorted into specific histograms.

To be able to sort events into separate beam pulse-on and beam pulse-off spectra, a signal was needed that could tell us when the beam was on and when the beam was off. Although Fig. 12 shows exactly such a signal, this signal was obtained from a beam stop. As such, this prevents the beam from reaching the target, making this signal unusable for the purposes of data acquisition. We contemplated using the signal shown in Fig. 10, but this voltage is used to drive the microwave source and does not directly indicate the pulse structure of the ion beam. This signal is also not useful because it assumes that powering the microwave

source *always* results in a beam pulse, which could fail to be the case on some occasions.

Between the ECR ion source and its old acceleration column, there existed a variable diameter collimator that was used to prevent divergent ion beam particles from entering the beam line [7]. In principle, during operation of the ECR accelerator, it is desirable to minimize, or completely eliminate, the current that strikes the collimator. In practice, however, it was difficult and sometimes impossible to completely eliminate this collimator current. Since the velocity of the protons in the ion beam together with the length of the beam-line translates into a time of flight that is much smaller than the hundreds-of-milliseconds time scale of the beam pulsing, it can be assumed that the ion beam is on target while the ion beam strikes the collimator.

Bret Carlin devised a circuit which took the analog signal of the collimator current, differentiated it to detect the rising and falling edges of the signal, and then used a Schmitt trigger to produce a digital signal that could be fed to one of the ADC channels of the DAQ. Jack Dermigny wrote the first version of the sort routine including ion beam pulsing, which was later revised by Christian Iliadis to include the capability for coincidence spectroscopy using LENA's NaI(Tl) detector annulus. This sort routine accepts the detector signals as well as the beam pulse-on signal from Bret Carlin's circuit. The latter signal, together with the master trigger of the coincidence spectrometer (which is provided by the HPGe signal), is fed into a logic coincidence module. Only when both signals occur simultaneously, i.e., the HPGe detector was triggered and the beam pulse is on, is an output pulse produced. This output is sorted into a histogram and the user can set a software gate (i.e., a sort condition) on the coincidence peak to select beam-on events only. Alternatively, the events can be sorted to select beam-off events only. The analysis of data recorded with a pulsed ion beam will be discussed in the next section.

IV. DATA ANALYSIS

The goal of this thesis is to compare the signal-to-noise ratio for two situations: (i) data accumulated using DC beam for a given total charge; and (ii) data accumulated with a pulsed beam of 10% duty cycle with an order of magnitude increase in beam intensity. This comparison sounds at first counter-intuitive. Why should one disregard 90% of the beam if a higher beam intensity clearly increases the signal-to-noise ratio, according to Eq. 1? It must

be remembered that we anticipate a beam intensity of 30 mA at LENA in the near future, and most beam-stop targets will not be able to withstand this current without significant degradation. Running with a pulsed proton beam of 30 mA and 10% duty cycle provides an *average* beam of 3 mA on target, similar to the current maximum DC beam intensity. However, and this is the crucial point, with a pulsed 30 mA beam the beam is effectively off for 90% of the time, i.e., the background is significantly reduced and a much higher signal-to-noise ratio can be achieved compared to the current setup.

Experimental setup

In order to test the efficacy of the beam pulsing system, we measured the γ-ray spectrum of a well-understood, strong resonance: the 151 keV resonance of the $^{18}\mathrm{O}(p,\gamma)^{19}\mathrm{F}$ reaction. Two spectra were collected at the on-resonance proton bombarding energy of 151 keV. A spectrum was collected with DC beam for 1049 seconds, and a spectrum was collected using a 10% duty cycle pulsed beam, also for 1049 seconds. The DC run had a beam current of 37 μA and the pulsed beam run had a maximum current of 370 μA. Additionally, DC and pulsed off-resonance runs (at 145 keV proton energy) were taken at the same current values as the on-resonance runs. The off-resonance runs lasted 3147 seconds. The off-resonance runs were used to measure the reduction in background counts.

Primary and secondary γ-ray decays and branching ratios

In general, low-energy nuclear reactions like those measured at LENA result in a particular excited state of the reaction's compound nucleus. This excited state then decays to the ground state through a number of γ-ray emissions. LENA's detectors collect these γ-rays and JAM displays a histogram of the number of γ-rays collected as a function of the "bin" into which they fall. The numerical value of the bin that the counts fall into is related (and for our purposes, linearly proportional) to the energy of the γ-ray detected for that count. Higher peak intensities correspond to more probable decay events.

The mass difference between the initial and final state of a nuclear reaction is called the reaction Q-value and can be denoted by Q_m. For the $^{18}\mathrm{O}(p,\gamma)^{19}\mathrm{F}$ reaction, $Q_m = 7994$ keV. Since this experiment has a laboratory proton beam energy of 151 keV, the added energy

of the proton in the center-of-mass system together with the Q-value leaves the ^{19}F nucleus in its 8140 keV ($J^{\pi} = \frac{1}{2}^{+}$) excited state. A primary γ-ray decay is any transition from this excited state to a lower energy level. Tilley et al. [11] identify seven primary γ-ray decays for this excited state of ^{19}F. Table I shows the literature values of branching ratios for these primary decays.

TABLE I: Primary branching ratios for the 8140 keV excited ($J^{\pi} = \frac{1}{2}^{+}$) state of ^{19}F; from Tilley [11].

Transition (final energies in keV)	Branching ratio (%)
R $\rightarrow$ 0	8 ± 1
R $\rightarrow$ 110	24 ± 2
R $\rightarrow$ 195	8 ± 1
R $\rightarrow$ 1553	2 ± 1
R $\rightarrow$ 3908	54 ± 2
R $\rightarrow$ 5944	1.0 ± 0.5
R $\rightarrow$ 6251	3 ± 1

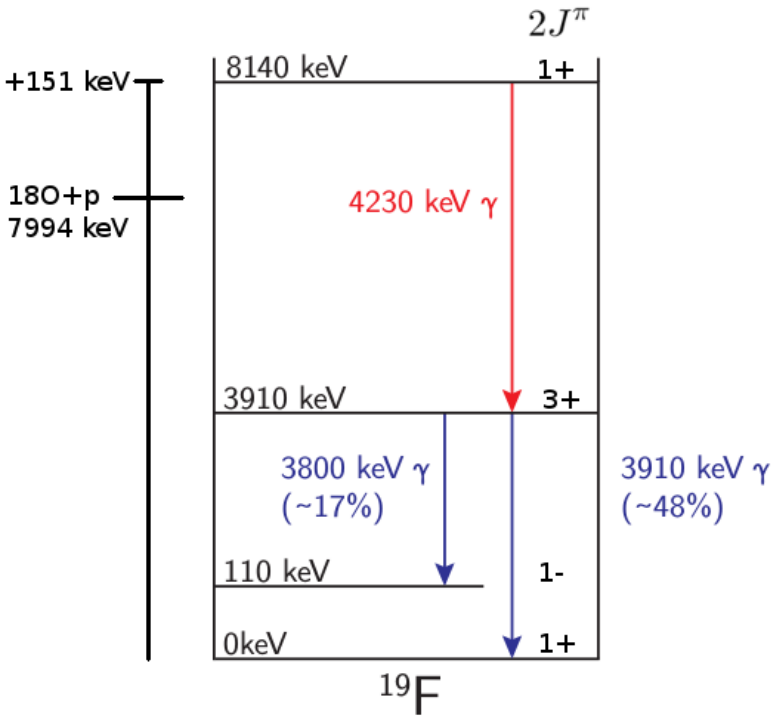

FIG. 14: An energy level diagram of ^{19}F showing one primary decay (in red) and two possible secondary decays (in blue).

Apart from the first transition in Table I that goes straight to the ground state by emitting a single 8140 keV γ-ray, all other primary transitions emit secondary γ-rays as they decay through various branches to the ground state. For example, the primary transition shown in Fig. 14 is the most probable primary decay branch, having a probability of $54 \pm 2\%$. Then, from the 3910 keV ($J^{\pi} = \frac{3}{2}^{+}$) state, there are four possible secondary decays. Figure 14 shows two possible secondary decays.

Fraction-fitting analysis

Analysis of the spectra was accomplished through a process called fraction-fitting that was only recently developed by the LENA group (see Buckner et al [4]). This process involves using GEANT4, a Monte Carlo simulation program, to generate simulated template spectra, which are then fit to the experimental spectrum using a program written in ROOT. The aim is to extract the primary branching ratios and total number of ^{18}O+p reactions that took place. This program uses the methods of Barlow and Beeston [3]. Files that replicate

the geometry of the LENA detectors and contain the secondary branching ratios from the literature (Tilley et al. [11]) have been created for use in GEANT4. With this input, the Monte Carlo calculations predict the detector response (i.e, the pulse height spectrum) for each simulated *primary* decay.

For this experiment, a total of eight templates were used in the fraction-fitting process. A background template spectrum was not simulated, but adopted from a 72179 second (approximately 20 hour) background run at LENA. Using GEANT4, one template spectrum was simulated for each of the seven primary decay branches using 2,000,000 ^{19}F decay (or, equivalently, ^{18}O+p reaction) events in each simulation. For example, the R $\rightarrow$ 1553 keV template was created by simulating the decay of ^{19}F from its 8140 keV excited state to the 1553 keV level, taking into account all possible secondary decays (for example, the most probable decay from this state is to the 195 keV state).

When running the ROOT fraction-fitting program, one must select the lower and upper limits of the fit, below and above which the program does not attempt to fit the templates to the spectrum. We ran the fraction-fitting program on the continuous beam spectrum, as well as the spectrum from the pulsed run that corresponded only to the counts collected while the beam was on. Let us call this spectrum the beam pulse-on spectrum. The lower limit for this experiment was chosen to be 450 keV, since below this limit there are poorly-understood detector hardware effects that are unaccounted for in the GEANT4 simulations. The upper limit was chosen to be 8160 keV, since there can be no γ-ray peaks from the reaction above this energy. The total number of experimental detector counts within this energy range is called the data area, and is denoted by A_{data}. For the continuous beam spectrum, $A_{data} = 77900$. For the beam pulse-on spectrum, $A_{data} = 64850$. Let us define the "fit area" of template spectrum i as the number of counts between the upper and lower fit bounds, and let us denote it with $A_{fit,i}$.

TABLE II: Fit areas for each of the primary-decay templates

Template	Fit area, $A_{fit,i}$
R $\rightarrow$ 0	312000
R $\rightarrow$ 110	309800
R $\rightarrow$ 195	312200
R $\rightarrow$ 1553	517400
R $\rightarrow$ 3908	555200
R $\rightarrow$ 5944	650000
R $\rightarrow$ 6251	519600

Table II shows the fit areas of each of the primary-decay templates except for the background template. It is not particularly useful to list the fit area for the background spectrum, because these counts do not come from the reaction.

The fraction-fitting program creates a linear combination of these templates that fits as closely to the experimental spectrum as possible by minimizing the χ^2 value. This method of γ-ray spectrum decomposition can be preferable to a conventional, by-hand analysis, since it fits the entire response function of the secondary decays to the spectrum rather than just individual peaks, as is the case with the conventional analysis. Fig. 15 shows a region of the beam pulse-on spectrum. It shows the experimental data shaded in red, and the fraction-fit spectrum in blue. Note that the peak farthest to the right has an energy of 4230 keV, which is associated with the R $\rightarrow$ 3908 keV transition shown in Fig. 14. The two peaks to the left of it are from the two secondary γ-ray decays also shown in Fig. 14.

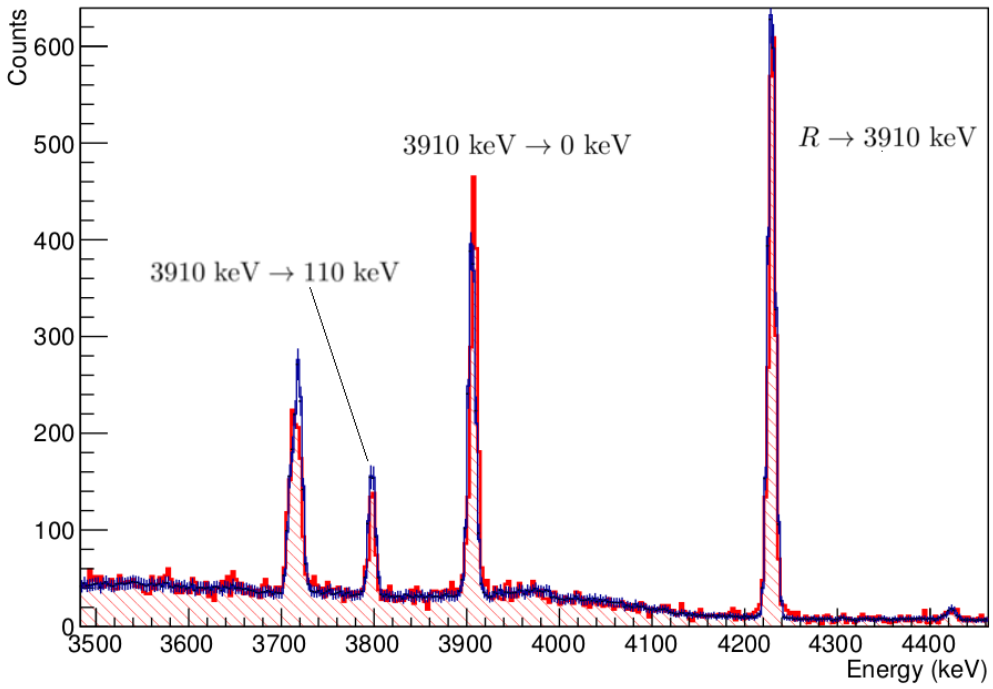

FIG. 15: A region of the beam pulse-on spectrum. The red shaded area is the experimental data, and the blue spectrum is the fitted spectrum created from the templates.The three peaks on the right show the same example transitions as in Fig. 14

Let us denote the fraction of the experimental spectrum which comes from the template spectrum i as f_i. Then the number of detected signals D_i solely caused by component i is given by

$$D_i = A_{data} \times f_i \tag{2}$$

We can compute the total number of reactions (irrespective of detector efficiencies) that decayed in primary branch i. Let us call this number N_i. Recall that the number of events in each GEANT4 simulation was N_{events} = 2,000,000. Then N_i is given by

$$N_i = \frac{D_i \times N_{events}}{A_{fit,i}} \tag{3}$$

For an excited state with n primary decay branches, the primary branching ratio BR_i for decay branch i can be computed by the following:

$$BR_i = \frac{N_i}{\sum_{i=1}^{n} N_i} \tag{4}$$

TABLE III: Fraction fitting results for DC beam spectrum

Template	Fraction, f_i	Detected signals, D_i	Number of reactions, N_i	Branching ratio (%)
Background	0.208 ± 0.003	16200 ± 200	N/A	N/A
R $\rightarrow$ 0	0.046 ± 0.003	3600 ± 200	23000 ± 1000	8.8 ± 0.5
R $\rightarrow$ 110	0.123 ± 0.003	9600 ± 200	62000 ± 2000	23.1 ± 0.6
R $\rightarrow$ 195	0.039 ± 0.003	3000 ± 200	19000 ± 1000	7.2 ± 0.5
R $\rightarrow$ 1553	0.006 ± 0.002	500 ± 100	1900 ± 600	0.7 ± 0.2
R $\rightarrow$ 3908	0.559 ± 0.004	43500 ± 300	157000 ± 1000	58.4 ± 0.7
R $\rightarrow$ 5944	0.008 ± 0.002	600 ± 200	2000 ± 500	0.7 ± 0.2
R $\rightarrow$ 6251	0.011 ± 0.001	800 ± 100	3300 ± 400	1.2 ± 0.2

TABLE IV: Fraction fitting results for beam pulse-on spectrum

Template	Fraction, f_i	Detected signals, D_i	Number of reactions, N_i	Branching ratio (%)
Background	0.040 ± 0.003	2600 ± 200	N/A	N/A
R $\rightarrow$ 0	0.060 ± 0.003	3900 ± 200	25000 ± 1000	9.2 ± 0.5
R $\rightarrow$ 110	0.149 ± 0.004	9600 ± 200	62000 ± 2000	22.9 ± 0.6
R $\rightarrow$ 195	0.052 ± 0.003	3400 ± 200	22000 ± 1000	7.9 ± 0.5
R $\rightarrow$ 1553	0.012 ± 0.002	800 ± 200	3100 ± 600	1.1 ± 0.2
R $\rightarrow$ 3908	0.663 ± 0.005	43000 ± 300	155000 ± 1000	56.9 ± 0.7
R $\rightarrow$ 5944	0.008 ± 0.002	500 ± 100	1600 ± 400	0.6 ± 0.2
R $\rightarrow$ 6251	0.015 ± 0.002	1000 ± 100	3700 ± 400	1.4 ± 0.2

Tables III and IV display f_i and D_i for each of the templates, as well as D_i, N_i, and BR_i for each of the primary decay branches. Table III is for the DC beam spectrum and table IV is for the beam pulse-on spectrum. The χ^2 value was 1.713 for fraction-fitting of the DC spectrum and was 1.733 for the beam pulse-on spectrum. The branching ratios in these tables are in agreement with the literature values from Tilley [11] in Table I, however the uncertainties in this experiment are greatly reduced. Table V shows that the uncertainties

for the each of the seven primary branching ratios decreased by between 50% and 80%. This reduction in uncertainty can be applicable as well. When determining the efficiency of a detector, it is valuable to have well-understood resonances. The 151 keV resonance of the $^{18}\mathrm{O}(p,\gamma)^{19}\mathrm{F}$ reaction is one such resonance. By having more precise branching ratios, detector efficiencies could be measured more precisely.

Furthermore, the branching ratios in Tables III and IV agree closely with one another. That is to say that the the beam pulsing method does not affect the values that are obtained for the branching ratios. Anything other than close agreement between these values would indicate serious issues with the validity of using the beam pulsing method for experiments.

TABLE V: Comparison of branching ratio uncertainties

Transition (final energies in keV)	Literature uncertainty (%) [11]	Experimental uncertainty (%)	Percent reduction in uncertainty
R $\rightarrow$ 0	1	0.5	50
R $\rightarrow$ 110	2	0.6	70
R $\rightarrow$ 195	1	0.5	50
R $\rightarrow$ 1553	1	0.2	80
R $\rightarrow$ 3908	2	0.7	65
R $\rightarrow$ 5944	0.5	0.2	60
R $\rightarrow$ 6251	1	0.2	80

It is a useful check of our procedure to verify that we did not lose very much information about the reaction itself when we performed our beam-pulsing. We can compute the total number of reactions per unit beam charge $\mathcal{N}$ by summing N_i for the seven primary decay branches and normalizing by the beam charge in the following way:

$$\mathcal{N} = \frac{\sum_{i=1}^{7} N_i}{q} \tag{5}$$

For the DC beam spectrum, the total number reactions, $\sum_{i=1}^{7} N_i$, was 268000 ± 3000, and the beam charge was $q_{DC} = 37661$ μC. For the pulsed beam, the total number of reactions was 272000 ± 3000, and the beam charge was $q_{pulse} = 38651$ μC. Then the percentage of reactions

lost in the beam pulsing procedure is given by

$$\%\text{ reactions lost in pulsing} = \left(1 - \frac{\mathcal{N}_{pulse}}{\mathcal{N}_{pulse}}\right) \times 100 = 1\% \tag{6}$$

Using the values of N_i from tables III and IV, as well as equations 5 and 6 shows us that the beam pulsing resulted in only a 1% loss in reactions compared to the ordinary DC procedure. This is very good news, because it shows that the ion beam pulsing procedure does not cause us to lose any significant amount of information about the reaction.

To verify that the ion beam pulsing method actually decreases the γ-ray counts from background sources, it is useful to examine the 1461 keV peak from environmental ^{40}K. This is purely a background peak, since there is no way that the reaction can produce a photon of this energy. Table VI shows net intensity of (or equivalently, the total counts in) this peak for the DC off-resonance run and the pulsed off-resonance run. The pulsed run has three different values for the peak intensity: one for the beam pulse-on histogram, one for the beam pulse-off histogram, and one for the Ge Singles histogram, which is the sum of the beam pulse-on and beam pulse-off histograms.

TABLE VI: Comparison of net intensity of the 1461 keV peak from environmental ^{40}K between runs.

DC	Pulsed		
	Ge Singles	Beam pulse-on	Beam pulse-off
1446 ± 42	1452 ± 43	150 ± 13	1322 ± 40

Table VI confirms that the beam pulse-on spectrum contained 10% of the background counts due to environmental ^{40}K when compared to the the Ge Singles spectrum. The beam pulse-off spectrum contained the remaining 90% of counts.

What can be concluded from these results is that the beam-pulsing method significantly reduces the background counts in the γ-ray spectra for this nuclear reaction without losing significant information about the reaction itself. Branching ratios produced with this pulsing method agree with values produced using DC beam, and are comparable to values cited in existing literature.

The implications of this result are rather significant. Although the 151 keV resonance of the $^{18}\mathrm{O}(p,\gamma)^{19}\mathrm{F}$ reaction is relatively strong, weaker resonances can benefit greatly from the

90% reduction in background counts. Pulsing will then greatly reduce the amount of time needed to run an experiment on a weak resonance in order to achieve the same statistical significance of the resulting spectrum when compared to a DC beam experiment. Because the method is the same irrespective of the type of target being used, every experiment utilizing the ECR ion source and accelerator can benefit from reduction in background counts due to this method.

V. SUMMARY AND FUTURE WORK

The goals of this thesis were the following:

- To design features of the ion beam transport system that would allow for a higher intensity beam and correct lossy beam transport
- To characterize the efficacy of the ion beam pulsing method using fraction-fitting analysis of the 151 keV resonance of the $^{18}\mathrm{O}(p,\gamma)^{19}\mathrm{F}$ reaction

The designs of the aforementioned beam-transport hardware have been physically realized. Currently, the hardware renovations of LENA's ECR accelerator and beam-line are under way. The solenoidal lenses have been installed in the beam-line, aligned, and have been connected to both water and current supplies. The beam stops have also been installed in the beam line, but the chilled, deionized water lines have not been attached, and the pneumatic tubing has not been connected to the actuator. The new acceleration column has been installed on the high voltage table, but further work is needed to test its high-voltage integrity and to install all the electronics needed to operate the pusled ECR source.

Testing of the beam-pulsing method using the 151 keV resonance of the $^{18}\mathrm{O}(p,\gamma)^{19}\mathrm{F}$ reaction has demonstrated that a 90% reduction in background counts is achievable, with a loss of only 1% in total reactions. This result serves as a proof-of-concept of the ion beam pulsing protocol. Ultimately, this procedure will be used in conjunction with the fully-upgraded ECR ion source and beam-transport system. The following hardware-related concerns will need to be tested before determining whether the upgrade was a success:

1. We must test the maximum current that can be extracted from the new column to see whether it matches or exceeds the factor-of-ten improvement as expected.

2. We must see that the beam stops function as expected with regard to their pneumatic actuation.

3. We must see that the cooling system of the beam stops protects them against the high current produced by the new column.

4. We must test that the beam stops make accurate current measurements.

5. We must test the solenoids to see whether they operate as expected and are able to fully focus the beam on the target.

6. It is not known whether complete elimination of collimator current will be easily achievable with the new acceleration column. Concerning the signal that the data acquisition system uses to separate the beam-on spectra from the beam-off spectra, it is desirable to look for a method which does not rely on current that strikes the collimator.

ACKNOWLEDGEMENTS

I would like to thank my advisors, Christian Iliadis and Tom Clegg for their guidance and support throughout my time at LENA. I would like to thank Mark Emamian for his suggestions in designing the beam-transport features, as well as Brian Walsh for assisting me in understanding and meeting the water-cooling needs of these features. I'd like to thank Bret Carlin for his assistance with LabView and the National Instruments hardware required for implementing the beam-pulsing, as well as his implementation of the circuitry required for gating the data acquisition software. I would especially like to thank Keegan Kelly and Jack Dermigny for their role in the data-taking and data analysis, without whom this project would lack substantive data.

---

[1] *FieldPoint: FP-1601 User Manual.*

[2] *FieldPoint Operating Instructions: FP-PG-522 and cFP-PG-522.*

[3] R. Barlow. Fitting using finite Monte Carlo samples. *Computer Physics Communications*, 77.

[4] M.Q. Buckner. High-intensity-beam study of ^{17}O(p,γ)^{18}F and thermonuclear reaction rates for ^{17}O+p. *Physical Review C*, 91(015812).

[5] M.Q. Buckner. Thermonuclear reaction rate of ^{18}O(p,γ)^{19}F. *Physical Review C*, 86.

[6] J. M. Cesaratto. Measurement of the $E_r^{c.m.}$=138 kev resonance in the ^{23}Na(p,γ)^{24}Mg reaction and the abundance of sodium in AGB stars. *Physical Review C*, 88(065806).

[7] J.M. Cesaratto. Nuclear astrophysics studies at LENA: The accelerators. *Nuclear Instruments and Methods in Physics Research A*, 623.

[8] A.E. Champagne. Nuclear astrophysics in the laboratory and in the universe. *AIP Advances*, 4.

[9] R. Longland. Nuclear astrophysics studies at the LENA facility: The γ-ray detection system. *Nuclear Intruments and Methods in Physics Research A*, 566.

[10] K.B. Swartz. A java-based data acquisition system for nuclear physics. *Nuclear Instruments and Methods in Physics Research A*, 463.

[11] D.R. Tilley. Energy levels of light nuclei A = 18-19. *Nuclear Physics A*, A595(1).